IEEE Access
Multidisciplinary ⋮ Rapid Review ⋮ Open Access Journal

Received May 10, 2022, accepted May 31, 2022, date of publication June 3, 2022, date of current version June 9, 2022.

Digital Object Identifier 10.1109/ACCESS.2022.3180156

Sensorless Position Estimation for Permanent Magnet Synchronous Linear Motor With Variable Coupling Length

LUHONG ZHANG, BINGRAN LI, PEIQING YE, CHUNLEI ZHANG, AND HUI ZHANG

Department of Mechanical Engineering, Tsinghua University, Beijing 100084, China
Beijing Key Laboratory of Precision/Ultra-Precision Manufacturing Equipment and Control, Tsinghua University, Beijing 100084, China

Corresponding author: Bingran Li (libingran1992@126.com)

This work was supported in part by the National Natural Science Foundation of China under Grant 51875312.

ABSTRACT Affected by the structure size of a permanent magnet synchronous linear motor, the coupling length of the mover and stator will change when the relative motion occurs. This paper analyzes the influence of the linear motor coupling length change on the position estimation accuracy of the position sensorless algorithm and proposes a Gauss-Newton iterative method to estimate the position. Compared with the existing high-frequency injection method, the proposed method is unaffected by the change of the coupling length, has strong robustness to the change of inductance parameters, and can obtain high position accuracy in the entire motion stroke. In this paper, the finite element method is used to analyze the variation law of the inductance parameter caused by the change of the coupling length, and the influence of the change of the inductance parameter on the position estimation accuracy of the position sensorless algorithm. The high-frequency differential current is obtained by the stationary reference frame high-frequency square-waveform injection method and difference processing, Moreover, the fast Fourier transform in the position domain is carried out to obtain the high-frequency differential current model function. The Gauss-Newton iterative method is used to obtain the estimated position of the linear motor in the entire motion stroke by estimating the position of each position sampling point. Lastly, the position accuracy of the proposed method and the traditional phase-locked loop method is compared and verified through experiments, and the corresponding conclusions are drawn.

INDEX TERMS High-frequency injection, Gauss-Newton iteration, sensorless, variable coupling linear motor.

I. INTRODUCTION

Permanent magnet synchronous linear motor (PMSLM) is mainly composed of the stator and mover. The stator mainly includes the winding coil and shell, and the mover includes the permanent magnet and mover iron. PMSLM has the advantages of simple structure, high efficiency, good dynamic performance, and direct driving load. It is widely used in the field of linear servo drives such as medical treatment, numerical control (NC) machine tools, and automatic machining [1]–[5]. The position feedback of the linear motor mainly includes the Hall sensor, grating sensor, and so on. These sensors can provide accurate position information to the linear motor, but they have the disadvantages of large space occupation and high cost. Therefore, sensorless methods have received increasing attention and studied in recent years to improve reliability, reduce cost, and reduce system volume.

Position sensorless technology mainly includes two methods: the fundamental frequency back electromotive force (EMF) method and the high-frequency injection method. The fundamental frequency back EMF method [6], [7] uses the fundamental frequency electromotive force of the motor [8], [9] and establishes an observer [10], [11] to obtain the position information of the rotor. This method is suitable for the motor in the high-speed motion region, it is difficult to estimate the rotor position at low speed, and it is not available at zero speed. Another method is the high-frequency injection method [12]–[14], this method is mainly used in medium and low-speed motion regions. The principle of which is to use the saliency characteristics of the motor.

The associate editor coordinating the review of this manuscript and approving it for publication was Dong Shen.

The high-frequency voltage is injected into the fundamental frequency voltage of the stator coil. After a coordinate transformation, rotor position information is included in the high-frequency current response, and the position of the rotor can be extracted by appropriate position demodulation.

For PMSLM, given that the coupling length changes with the movement of the mover, inductance parameters change, thereby making the sensorless position estimation accuracy change substantially. This is a problem that needs to be studied in depth.

At present, many scholars have carried out research on the sensorless algorithm for PMSLM. The inductance unbalance characteristics of the three-phase linear motor and the relationship between the inductance and the thrust are quantitatively analyzed, and a three-stage primary modular structure is proposed to improve the inductance unbalance and suppress the thrust fluctuation in [2]. Inductance characteristics of the two-phase cylindrical permanent magnet synchronous linear motor were analyzed using the finite element method, and the actual inductance parameters of the full coupling stage were introduced into the stationary reference frame high-frequency square-waveform injection algorithm. The extended Kalman filter (EKF) extracts the rotor position and realizes the position detection of the mover in [15]. In [16], flux linkage and inductance characteristics of the TPMSLM in the entire range of motion were analyzed. Inductance and flux linkage expressions of the entire coupling region were established using analytical methods and were verified by finite element and experimental tests. The preceding studies have carried out a series of investigations on the inductance parameters and position detection accuracy of the PMSLM. How to improve the position observation accuracy of the linear motor in the entire coupling stage still needs to be deeply studied.

In this paper, given the large position estimation error of the traditional high-frequency injection sensorless algorithm caused by the change in the linear motor coupling process, a Gauss-Newton iterative position estimation algorithm is proposed to perform high-frequency differential current modeling and position estimation to improve the linear motor. This method is not sensitive to the change of the inductance parameters and can still obtain high position estimation accuracy when the coupling length of the linear motor changes. The remainder of this paper is structured as follows. In the second section, the high-frequency square-waveform injection method of the stationary reference frame is analyzed, and the Gauss-Newton iterative method is proposed to demodulate the position of the linear motor mover. In Section III, inductance characteristics of the linear motor are simulated and analyzed, the high-frequency differential current curve modeling is carried out by fast Fourier transform (FFT) and the simulation analysis of position extraction is carried out by Gauss-Newton iteration. Section IV compares the proposed method with traditional sensorless position estimation methods through experiments. Lastly, Section V provides the corresponding conclusions.

II. SENSORLESS ALGORITHM

A. STATIONARY REFERENCE FRAME HIGH-FREQUENCY SQUARE-WAVEFORM INJECTION METHOD

Permanent magnet synchronous motor (PMSM) in the synchronous reference frame can be expressed by (1):

$$\begin{bmatrix} u_d \\ u_q \end{bmatrix} = \begin{bmatrix} R & -\omega_e L_q \\ \omega_e L_d & R \end{bmatrix} \cdot \begin{bmatrix} i_d \\ i_q \end{bmatrix} + \begin{bmatrix} L_d & 0 \\ 0 & L_q \end{bmatrix} \cdot p \begin{bmatrix} i_d \\ i_q \end{bmatrix} + \begin{bmatrix} 0 \\ \omega_e \psi_f \end{bmatrix} \tag{1}$$

where u_q and u_d are the stator voltage components, i_d and i_q are the stator current components, respectively, R is the stator winding resistance, L_d and L_q are the stator inductance components, ω_e is the mover electrical angular velocity, ψ_f is the permanent magnet flux linkage, and P is the differential operator.

The sensorless algorithm of high-frequency square-waveform injection aims to increase the frequency of the injected voltage to the order of PWM switching frequency. At this time, the linear motor can be regarded as a purely inductive circuit, so the partial pressure caused by high-frequency impedance can be disregarded [17]. The high-frequency voltage equation in the synchronous reference frame is as follows:

$$\begin{bmatrix} u_{dh} \\ u_{qh} \end{bmatrix} = \begin{bmatrix} L_{dh} & 0 \\ 0 & L_{qh} \end{bmatrix} \cdot p \begin{bmatrix} i_{dh} \\ i_{qh} \end{bmatrix} \tag{2}$$

where u_{dh} and u_{qh} are the high-frequency voltages of the d-axis and q- axis, L_{dh} and L_{qh} are the d- axis and q- axis inductances, i_{dh} and i_{qh} are the high-frequency currents of the d- axis and the q- axis, respectively.

The high-frequency voltage equation of the synchronous reference frame is transformed into the stationary reference frame through the coordinate transformation matrix, which can be derived as

$$\begin{bmatrix} u_{\alpha h} \\ u_{\beta h} \end{bmatrix} = \boldsymbol{T}_{r/s}(\theta) \cdot \begin{bmatrix} L_{dh} & 0 \\ 0 & L_{qh} \end{bmatrix} \cdot \boldsymbol{T}_{s/r}(\theta) \cdot p \begin{bmatrix} i_{\alpha h} \\ i_{\beta h} \end{bmatrix} \tag{3}$$

where $u_{\alpha h}$ and $u_{\beta h}$ are the high-frequency voltages of the $\alpha-$ axis and $\beta-$ axis, $i_{\alpha h}$ and $i_{\beta h}$ are the high-frequency currents of the $\alpha-$axis and $\beta-$ axis, respectively, θ is the electrical angle position. $\boldsymbol{T}_{r/s}(\theta)and\boldsymbol{T}_{s/\mathrm{r}}(\theta)$ is the transformation matrix between the synchronous and stationary reference frames, which is

$$\boldsymbol{T}_{r/s}(\theta) = \boldsymbol{T}_{s/r}^{-1}(\theta) = \begin{bmatrix} \cos\theta & -\sin\theta \\ \sin\theta & \cos\theta \end{bmatrix} \tag{4}$$

According to (4), the high-frequency current equation of the stationary reference frame can be represented as follows:

$$p \begin{bmatrix} i_{\alpha h} \\ i_{\beta h} \end{bmatrix} = \boldsymbol{M}(\theta) \cdot \begin{bmatrix} u_{\alpha h} \\ u_{\beta h} \end{bmatrix} \tag{5}$$

where $\boldsymbol{M}(\theta)$ is the inverse matrix of inductance matrix, which is expressed as

$$\boldsymbol{M}(\theta) = \begin{bmatrix} L_p + L_s \cos 2\theta & L_s \sin 2\theta \\ L_s \sin 2\theta & L_p - L_s \cos 2\theta \end{bmatrix} \tag{6}$$

where the coefficients L_p and L_s in the matrix $\boldsymbol{M}(\theta)$ are expressed as follows:

$$L_p = \frac{1}{2}\left(\frac{1}{L_{dh}} + \frac{1}{L_{qh}}\right), \quad L_s = \frac{1}{2}\left(\frac{1}{L_{dh}} - \frac{1}{L_{qh}}\right) \tag{7}$$

The high-frequency square-waveform injection method of the stationary reference frame is to inject a high-frequency voltage signal into the α-axis. The amplitude of the high-frequency square-waveform voltage in two adjacent PWM cycles is equal and the sign is opposite. The equation is as follows:

$$\boldsymbol{V}_{inj} = \begin{bmatrix} u_{\alpha h} \\ u_{\beta h} \end{bmatrix} = \begin{cases} \begin{bmatrix} +V_h \\ 0 \end{bmatrix}, & PWM1 \\ \begin{bmatrix} -V_h \\ 0 \end{bmatrix}, & PWM2 \end{cases} \quad (V_h > 0) \tag{8}$$

where $\boldsymbol{V}_{inj}$ is the high-frequency voltage, and V_h is the amplitude of the injected high-frequency voltage.

Thereafter, (8) is brought into (5), and the discretized high-frequency current differential equation can be derived as follows:

$$\begin{bmatrix} \Delta i_{\alpha h} \\ \Delta i_{\beta h} \end{bmatrix} = \text{sign}(u_{\alpha h}) \cdot \Delta T \cdot V_h \cdot \begin{bmatrix} L_p + L_s \cos 2\theta \\ L_s \sin 2\theta \end{bmatrix} \tag{9}$$

From the (9), there is a DC offset L_p in the high-frequency differential current equation of the α- axis, and the α- and β- axes contain the second harmonic related to position. In addition, the amplitudes of the expression related to the position θ are equal in the high-frequency differential current equations of the $\alpha-$ and β- axes.

B. HIGH-FREQUENCY DIFFERENTIAL CURRENT

From the derivation process of the preceding static axis high-frequency square-waveform sensorless method, the high-frequency differential current contains the mover position information. Moreover, the high-frequency differential current is affected by the injected high-frequency voltage amplitude and inductance parameters. The object of this study is the tubular permanent magnet synchronous linear motor (TPMSLM), and its related characteristics are relatively different from the permanent magnet synchronous rotating motor [8]. The TPMSLM is mainly composed of the stator and the mover. In particular, the stator includes the two-phase windings and the stator iron and belongs to a motor with a slotless structure. The mover includes the permanent magnet and the mover iron, and the magnetization direction of the permanent magnet is axial magnetization. The simplified structure of TPMSLM is shown in Fig. 1.

To extract the high-frequency differential current of PMSLM, the high-frequency voltage equation in the stationary reference frame is first expressed as follows:

$$\begin{bmatrix} u_{\alpha h} \\ u_{\beta h} \end{bmatrix} = \boldsymbol{M}^*(\theta) \cdot p \begin{bmatrix} i_{\alpha h} \\ i_{\beta h} \end{bmatrix} \tag{10}$$

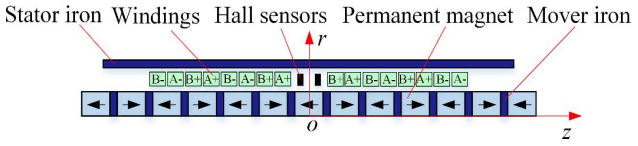

FIGURE 1. Schematic of TPMLSM.

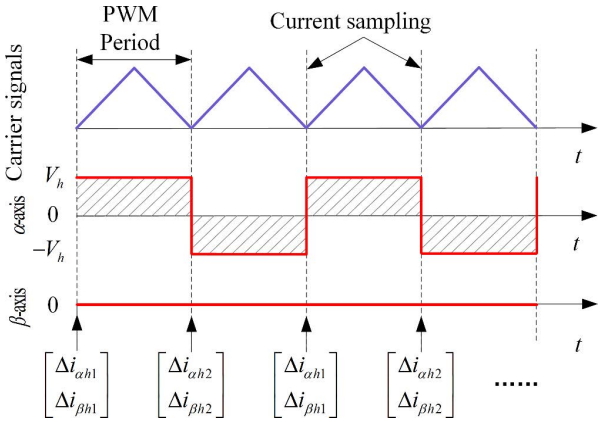

FIGURE 2. High-frequency square-waveform sensorless injection method in two PWM cycles block diagram.

where $\boldsymbol{M}^*(\theta)$ is expressed as the actual inductance matrix [18] of the stationary reference frame as follows:

$$\begin{aligned} \boldsymbol{M}^*(\theta) &= \begin{bmatrix} L_{\alpha h} & L_{\alpha\beta h} \\ L_{\alpha\beta h} & L_{\alpha h} \end{bmatrix} \\ &= \begin{bmatrix} L_1 - L_2 \cos 2\theta & L_3 - L_4 \sin 2\theta \\ L_3 - L_4 \sin 2\theta & L_1 + L_2 \cos 2\theta \end{bmatrix} \end{aligned} \tag{11}$$

Bringing the actual inductance matrix (11) into the differential current equation in (5), the derivation results are as follows:

$$p \begin{bmatrix} i_{\alpha h} \\ i_{\beta h} \end{bmatrix} = \boldsymbol{M}^*(\theta)^{-1} \cdot \begin{bmatrix} u_{\alpha h} \\ u_{\beta h} \end{bmatrix} \tag{12}$$

where

$$\boldsymbol{M}^*(\theta)^{-1} = \frac{1}{A} \cdot \begin{bmatrix} -L_1 + L_2 \cos 2\theta & L_3 + L_4 \sin 2\theta \\ L_3 + L_4 \sin 2\theta & -L_1 - L_2 \cos 2\theta \end{bmatrix} \tag{13}$$

$$\begin{aligned} A = &-L_1^2 + L_3^2 + L_2^2 \cos^2 2\theta + L_4^2 \sin^2 2\theta \\ &- 2L_3 L_4 \sin 2\theta \end{aligned} \tag{14}$$

Fig. 2 shows the block diagram of the high-frequency square-waveform sensorless injection method for two PWM cycles. In particular, high-frequency voltage with equal amplitude but the opposite symbol is injected into α- axis in two adjacent PWM cycles, In addition, the differential value of high-frequency current of the α- and $\beta-$ axes are obtained through current sampling.

The differential expression of the acquired high-frequency current in two adjacent PWM cycles can be represented as follows.

The high-frequency current differential term of the stationary reference frame in the first PWM cycle is expressed

as follows:

$$\begin{bmatrix} \Delta i_{\alpha h1} \\ \Delta i_{\beta h1} \end{bmatrix} = \frac{\Delta T \cdot V_h}{A} \cdot \begin{bmatrix} L_1 - L_2 \cos 2\theta \\ -L_3 - L_4 \sin 2\theta \end{bmatrix} \tag{15}$$

The high-frequency current differential term of the stationary reference frame in the second PWM cycle is expressed as follows:

$$\begin{bmatrix} \Delta i_{\alpha h2} \\ \Delta i_{\beta h2} \end{bmatrix} = \frac{\Delta T \cdot V_h}{A} \cdot \begin{bmatrix} -L_1 + L_2 \cos 2\theta \\ L_3 + L_4 \sin 2\theta \end{bmatrix} \tag{16}$$

The difference operation is performed on the high-frequency differential current obtained from two adjacent PWM cycles, and the results are as follows:

$$\begin{aligned} \begin{bmatrix} \Delta i^*_{\alpha h} \\ \Delta i^*_{\beta h} \end{bmatrix} &= \begin{bmatrix} \Delta i_{\alpha h1} - \Delta i_{\alpha h2} \\ \Delta i_{\beta h1} - \Delta i_{\beta h2} \end{bmatrix} \\ &= \frac{\Delta T \cdot V_h}{A} \cdot \begin{bmatrix} 2L_1 - 2L_2 \cos 2\theta \\ -2L_3 - 2L_4 \sin 2\theta \end{bmatrix} \end{aligned} \tag{17}$$

Equation (17) includes the DC offset and second harmonic components. After removing the DC offset part, it can be deduced as follows:

$$\begin{bmatrix} \Delta i^{**}_{\alpha h} \\ \Delta i^{**}_{\beta h} \end{bmatrix} == -2\Delta T \cdot V_h \cdot \begin{bmatrix} \frac{L_2}{A} \cdot \cos 2\theta \\ \frac{L_4}{A} \cdot \sin 2\theta \end{bmatrix} \tag{18}$$

After removing the DC offset, the high-frequency differential current equation only contains the second harmonic related to the position. However, the coefficient of the equation is composed of the inductance parameters of TPMSLM, and the preceding inductance parameters also change with the position. Therefore, the position error proposed by the traditional arctangent method or phase-locked loop (PLL) method will have a large position estimation error.

C. DEMODULATE THE MOVER POSITION OF LINEAR

In the process of mover position demodulation, to improve the accuracy of position estimation, this paper proposes the Gauss-Newton iterative method for position estimation and compares it with the traditional PLL method.

1) PLL METHOD

A traditional method for extracting the mover position is the PLL method [19], which consists of a proportional-integral (PI) controller and integrator, which can convert input error signal into a position signal. In this process, harmonic interference can be eliminated, and the speed and position information can be output. The high-frequency differential currents and the second harmonic of the output position are calculated by difference, and the result is used as the input of PLL. Thereafter the position estimate can be obtained. The block diagram of the mover position demodulation of the PLL method is shown in Fig. 3.

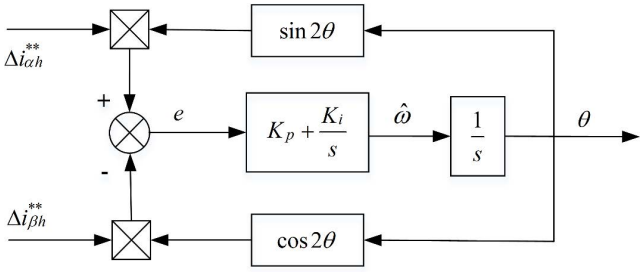

FIGURE 3. Block diagram of mover position demodulation for PLL method.

2) GAUSS-NEWTON ITERATIVE METHOD

The method of arctangent or PLL can obtain the position of the mover. However, the length of the mover for TPMSLM is higher than the stator length. In the actual moving process, if the running displacement is large, then the mover and stator will be partially decoupled stage. Therefore, the coupling relationship between the mover and stator during the linear motor motion is divided into two forms, namely, full and partial couplings, in which partial coupling includes left and right partial couplings.

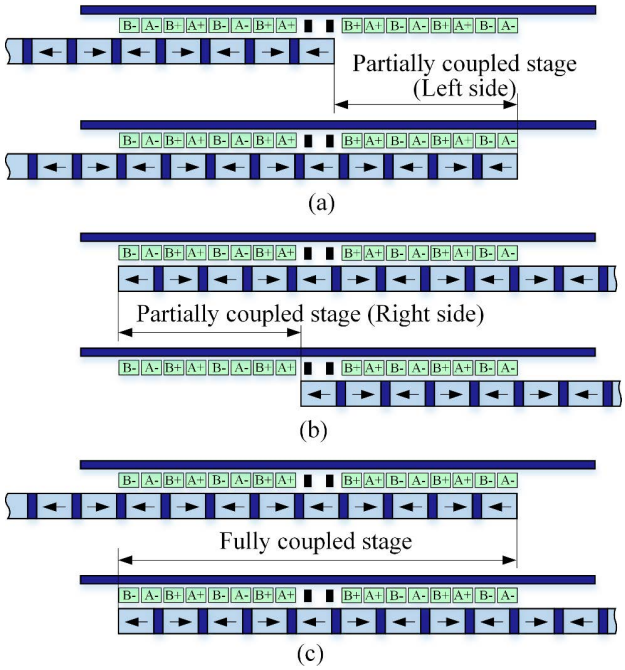

FIGURE 4. Schematic diagram of different coupling stages of PMSLM stator and mover (a: partially coupled stage - left side, b: partially coupled stage - right side, c: fully coupled stage).

As shown in Fig. 4, the coupling length of the stator and mover in the full coupling stage has a length of 9 pole pitches as the motor moves left or right, the coupling length gradually decreases. At the end of the mover moving to the edge of the Hall sensors, the coupling length is reduced from 9 pole pitches to 5 pole pitches. Compared with the traditional rotating PMSM, the change of electrical parameters will be

considerably complicated. In the partial coupling process, with the decrease of the coupling length of the mover and the stator, self and mutual inductance in the inductor will experience DC offset and attenuation of the second harmonic amplitude, which makes the position extraction markedly difficult [20].

The high-frequency differential current coefficient is composed of the motor's self and mutual inductance parameters. When the inductance parameter changes substantially, it will directly affect the accuracy of the position estimation. The high-frequency differential current is no longer a pure sinusoidal variation law in the entire motion stroke, but a polynomial form containing numerous harmonic components. In this case, the PLL method is no longer applicable. Therefore, this paper proposes an iterative method to estimate the position of the linear motor.

First, the actual spectral distribution of the high-frequency differential current is obtained through FFT, and then the polynomial function of the high-frequency current curve is established as follows:

$$\begin{aligned} \boldsymbol{f}(\mathrm{x}) &= \begin{bmatrix} f_A(x) \\ f_B(x) \end{bmatrix} \\ &= \begin{bmatrix} A_0 + \sum_k A_k \cos(2\pi \cdot \omega_{Ak} \cdot x/l + \varphi_{Ak}) \\ B_0 + \sum_k B_k \cos(2\pi \cdot \omega_{Bk} \cdot x/l + \varphi_{Bk}) \end{bmatrix} \end{aligned} \tag{19}$$

where $f_A(x)$ and $f_B(x)$ are the differential currents of the two-phase TPMSLM, A_0 and $B_0$are the DC offsets, A_k and B_k represent the harmonic amplitudes, ω_{Ak} and ω_{Bk} represent the harmonic frequencies, l is the pole distance, x is the displacement, φ_{Ak} and φ_{Bk} are the phase offsets.

Thereafter, the nonlinear least squares method is used to minimize the sum of squares of the residual values of the two phases. This function is used as the objective function of the iterative method, which is expressed as follows:

$$F(\mathrm{x}) = \frac{1}{2}(f_A(x) - f_{A\mathrm{m}}(x))^2 + \frac{1}{2}(f_B(x) - f_{B\mathrm{m}}(x))^2 \tag{20}$$

where $f_{A\mathrm{m}}(x)$ and $f_{B\mathrm{m}}(x)$ are the measured data of high-frequency differential currents.

The Jacobian matrix $\boldsymbol{J}_{AB}(x)$ is derived as follows:

$$\boldsymbol{J}_{AB}(x) = \begin{bmatrix} f'_A(x) \\ f'_B(x) \end{bmatrix} \tag{21}$$

The measured value function matrix $\boldsymbol{f}_m(x)$ of the high-frequency differential currents is shown as follows:

$$\boldsymbol{f}_m(x) = \begin{bmatrix} fA_m(x) \\ fB_m(x) \end{bmatrix} \tag{22}$$

The iteration step h_k of the Gauss-Newton method can be calculated as follows:

$$h_k = -\boldsymbol{J}^{\mathrm{T}}(\boldsymbol{f}(x_k) - \boldsymbol{f}_m(x_k))/(\boldsymbol{J}^{\mathrm{T}}\boldsymbol{J}) \tag{23}$$

Lastly, the iterative estimation of mover position is carried out, which is expressed as follows:

$$x_{k+1} + h_k = x_k \tag{24}$$

$$x_{k+1} = x_k - \boldsymbol{J}^{\mathrm{T}}(\boldsymbol{f}(x_k) - \boldsymbol{f}_m(x_k))/(\boldsymbol{J}^{\mathrm{T}}\boldsymbol{J}) \tag{25}$$

For a TPMSLM, the initial value is $x_0 = 0$, Thereafter, the stator position is obtained using one-step Gauss-Newton iteration method. This position is used as the initial value of the next iteration, and the position iteration of the next sampling point is performed. The specific iterative process is shown in Fig. 5.

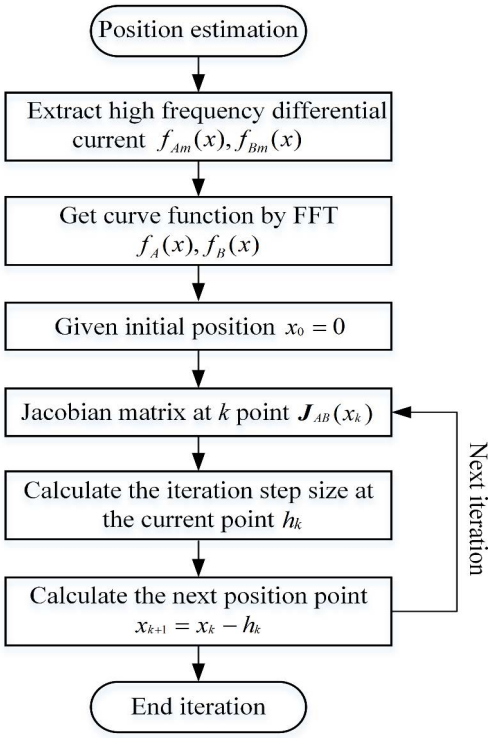

FIGURE 5. Gauss-Newton iterative estimation flow diagram.

III. SIMULATION ANALYSIS OF POSITION ESTIMATION

A. TPMSLM INDUCTANCE PARAMETER SIMULATION

Given that the characteristics of self and mutual inductance directly determine the amplitude of the high-frequency differential current, this chapter firstly simulates and analyzes the inductance characteristics of the linear motor. The PMSLM structural simulation model shown in Fig. 1 is established by ANSYS Maxwell software, and the material properties of each part are set according to Table 1. Inductance parameter simulation under different coupling lengths is carried out according to the relative positions of the stator and mover shown in Fig. 2. This paper takes the zero-phase point of the mover near the middle position of the stator as the center position, and the distance of 30 mm before and after is used as the full range of motion. That is, the motion displacement is 60 mm. Self-inductance and mutual inductance parameters after simulation are shown in Fig. 6.

The simulation results in Fig. 6 show that the self and mutual inductance of the AB phase are sinusoidal curves, and there are DC offsets and second harmonics related to the position. This variation law is markedly consistent with Equation (11). In all the intermediate coupling stages, as shown

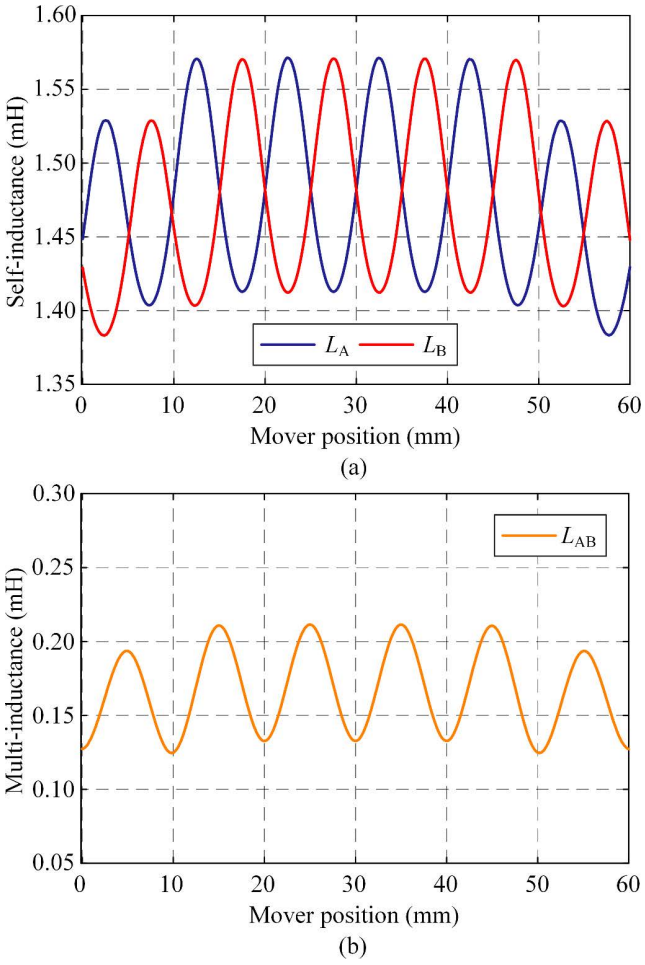

FIGURE 6. Simulation results of variation of inductor parameters: self-inductance (a), mutual inductance (b).

in Fig. 4(c), the self-induced DC offset and the amplitude of the second harmonic remain unchanged. Meanwhile, in some coupling stages, as shown in Fig. 4(a) and (b), the amplitude of the DC offset and the second harmonic will attenuate to varying degrees. If the mover position is obtained by using the position demodulation process in the traditional high-frequency square-waveform injection algorithm, then a large position estimation error will occur in some coupling stages.

B. OBTAIN HIGH-FREQUENCY CURRENT CURVE PARAMETERS

The simulation results in the previous chapters show that because the inductance parameters of PMSLM directly constitute the amplitude of high-frequency differential currents and its value changes with the position of the mover, the complex inductance parameters will directly affect the accuracy of sensorless position estimation.

The high-frequency differential current mainly includes fundamental frequency and second harmonic components. Therefore, based on the inductance simulation results and measured high-frequency differential current, a preliminary simulation model can be established to preliminarily verify the effectiveness of the Gauss-Newton position iteration algorithm.

Specific data in the simulation process include the fundamental frequency and second harmonic parameters of the two-phase high-frequency differential current model of linear motor:

$$\begin{aligned} \boldsymbol{f}_{sim}(\mathrm{x}) &= \begin{bmatrix} f_A^{sim}(x) \\ f_B^{sim}(x) \end{bmatrix} \\ &= \begin{bmatrix} A_0 + A_1 \cos(2\pi \cdot \omega_{A1} \cdot x/L + \varphi_{A1}) \\ B_0 + B_1 \cos(2\pi \cdot \omega_{B1} \cdot x/L + \varphi_{B1}) \end{bmatrix} \end{aligned} \tag{26}$$

The parameters represent the simulation values in Equation (26). In particular $f_A^{sim}(x)$ and $f_B^{sim}(x)$ are the differential currents of the two-phase TPMSLM, A_0 and $B_0$are the DC offsets, A_1 and B_1 represent the harmonic amplitudes of the second harmonic, ω_{A1} and ω_{B1} represent the harmonic frequencies, l is the pole distance, x is the displacement, and φ_{A1} and φ_{B1} are the phase offsets of the second harmonic.

To verify the effectiveness of the adopted Gauss-Newton iterative position estimation algorithm, random noise $\boldsymbol{v}_{random}$ is added based on the simulation model to simulate the measured value of high-frequency differential current, as shown in (27):

$$\boldsymbol{f}_m^{sim}(x) = \boldsymbol{f}_m^{sim}(x) + \boldsymbol{v}_{random} \tag{27}$$

Parameters used in the simulation model are shown in Table 1.

TABLE 1. Simulation parameters for the high-frequency differential current models.

Phase	Harmonics	Fundamental frequency	Double frequency
A	Amplitude	1.16 A	0.06 A
	Phase angle	0°	15°
B	Amplitude	0.10 A	0.03 A
	Phase angle	180°	-75°

Fig. 7 shows the phase AB model curve of high-frequency differential current and simulated data. Fig. 8 shows the theoretical and iterative estimates of position estimates. Fig. 9 shows the Gauss-Newton iterative position estimation error. Fig. 7, Fig. 8, and Fig. 9 are simulation curves, the abscissa coordinate is the position, which represents the displacement of the motor movement, and its maximum value is 60 mm. This process is consistent with the displacement of the linear motor in the subsequent experiments.

IV. EXPERIMENTAL VERIFICATION

The sensorless position estimation method proposed in this paper is verified by a PMSLM single-axis experimental platform, as shown in Fig. 10. The control system of the experimental platform is built based on TI's TMS320F28335 digital processing chip. The linear motor adopts a two-phase cylindrical PMSLM. The bus voltage of the linear motor

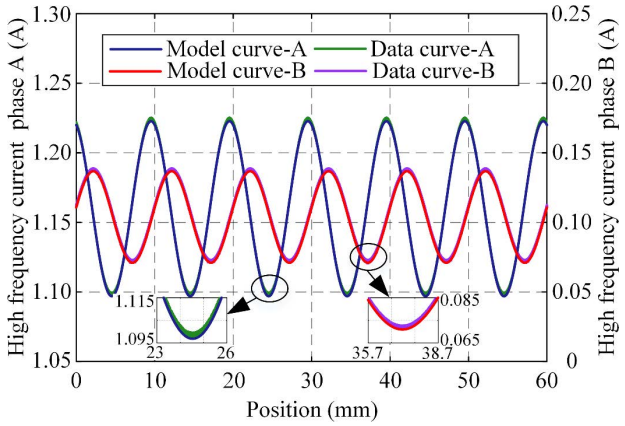

FIGURE 7. High-frequency differential current simulation curve.

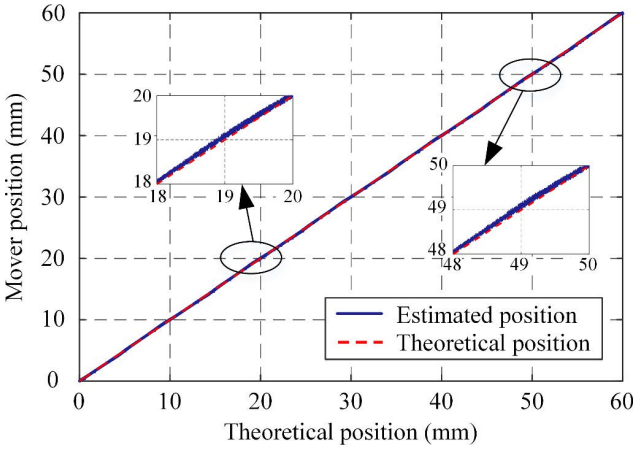

FIGURE 8. Simulation values and theoretical values of position estimation.

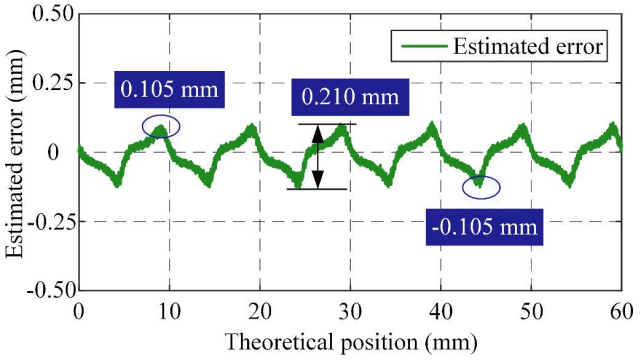

FIGURE 9. Gauss-Newton iterative position estimation error.

is 48 V, the current sampling frequency is 20 kHz, the high-frequency injection voltage is 16V and the injection frequency is 10 kHz. The inductance parameters are measured by the LCR bridge, and the grating sensor is used as the sensor for position calibration.

The structure of the linear motor is shown in Fig. 11, and the detailed dimensions are shown in Table 2.

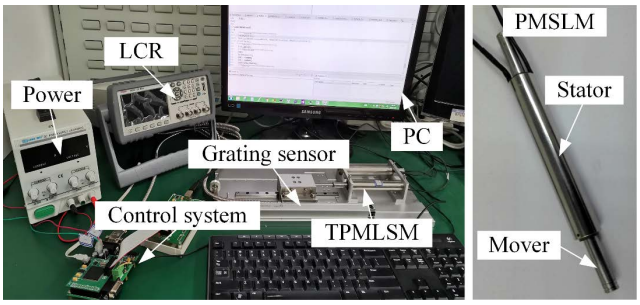

FIGURE 10. Single-axis experimental platform.

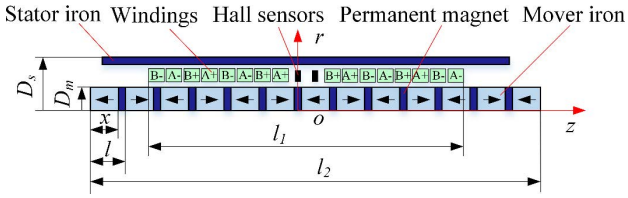

FIGURE 11. PMSLM structural parameters.

TABLE 2. Linear motor size parameters.

Symbol	Harmonics	Fundamental frequency
l_1	Coil length	89.5 mm
l_2	Mover length	130 mm
x	Permanent magnet length	8 mm
D_s	Stator diameter	18 mm
D_m	Mover diameter	10 mm
l	Pole distance	2 mm
n	Number of permanent magnets	13
N	Coil winding turns	100

A. MEASURED INDUCTANCE VALUE

For the cylindrical PMSLM in this paper, the self-inductance and mutual inductance parameters can be measured through the LCR bridge. The self-inductance coefficient can be measured directly through the bridge, and the mutual inductance value can be measured indirectly: (1) connect the AB phases of the motor in forward and reverse series to measure the value, and (2) process the difference between the two sets of data, and 1/4 of the difference is the mutual inductance value we want to obtain [21].

Fig. 12(a) and Fig. 12(b) are the self-inductance and mutual inductance values measured by this method, respectively. As shown in Fig. 12, inductance value measured by the LCR bridge has a deviation of about 5% compared with the simulation results. This result may be caused by machining and assembly errors of PMSLM. However, the results of the finite element simulation and measured value have the same variation law with the mover position.

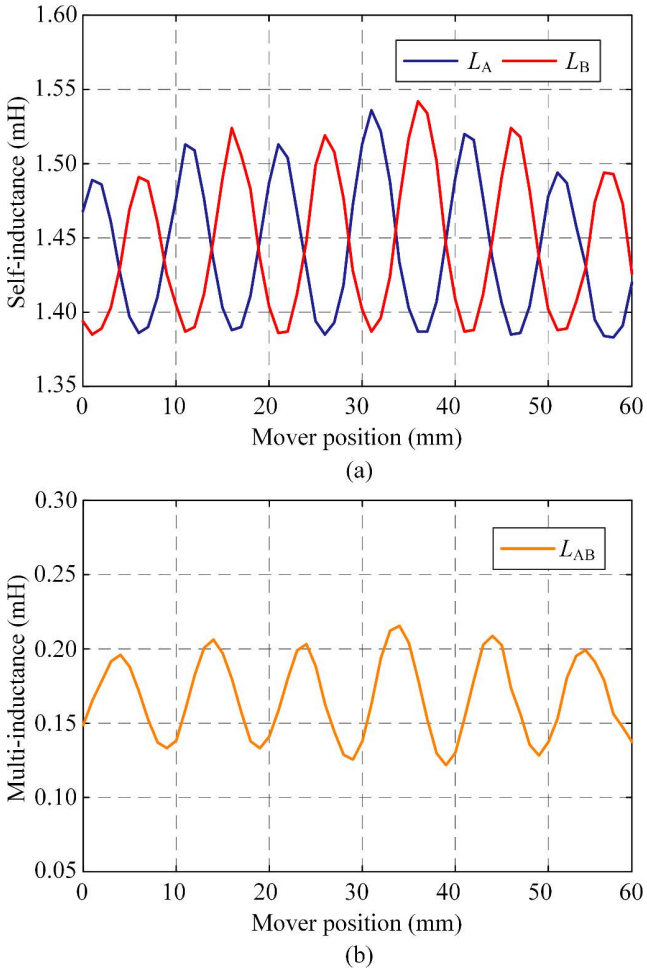

FIGURE 12. Measured results of changes: self-inductance (a) and mutual inductance (b).

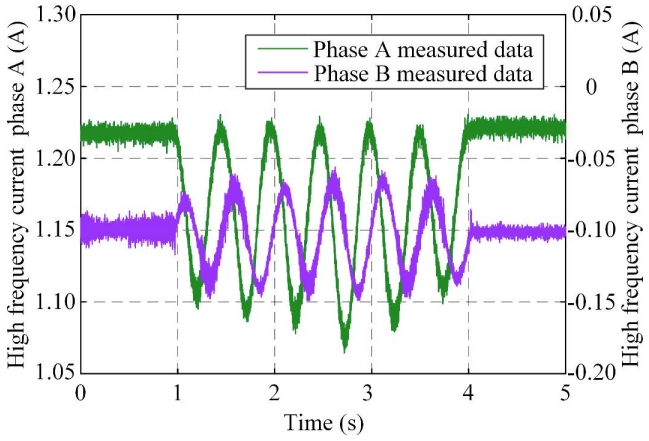

FIGURE 13. High-frequency differential current (maximum speed: 20 mm/s).

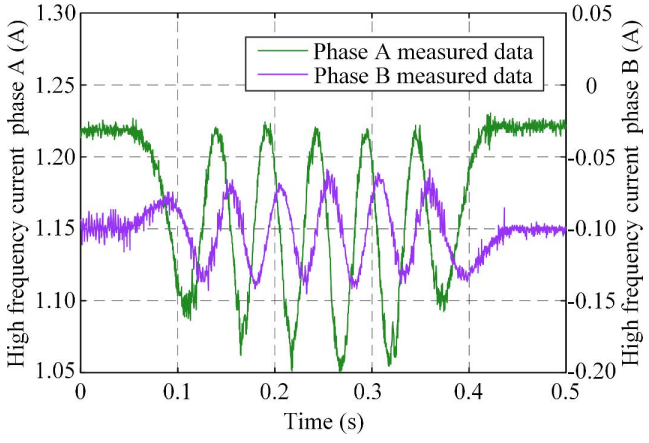

FIGURE 14. High-frequency differential current (maximum speed: 200 mm/s).

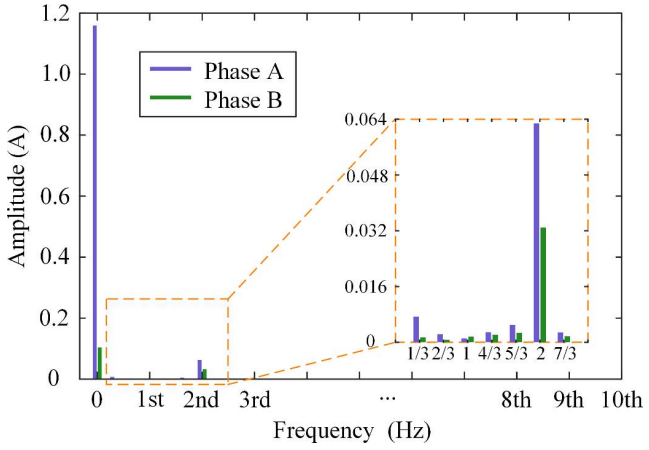

FIGURE 15. Phase A and B differential current FFT spectrum (maximum speed: 20 mm/s).

B. ESTABLISH HIGH-FREQUENCY DIFFERENTIAL CURRENT CURVE MODEL FUNCTION

The preceding analysis indicates that the high-frequency differential current obtained by the high-frequency square-waveform injection method includes DC offset and position-related second harmonic. Moreover, and the amplitude of the second harmonic is mainly affected by the self-inductance and mutual inductance parameters of the linear motor itself.

Position error experiment in this paper verifies the proposed position estimation method under two different maximum speeds. Fig. 13 and Fig. 14 show the high-frequency differential current curves at the maximum speeds of 20 mm/s and 200 mm/s, respectively. The experimental procedure is as follows:

a. Single-axis experimental platform shown in Fig. 10 was used in this experiment. Take the 0 electrical angle point shown in Fig. 11 as the middle point of the movement, and take the point back 30 mm as the starting point of the movement.

b. In the current loop of the servo system, we injected high-frequency voltage signals with equal amplitudes but opposite symbols into the α- axis in the stationary reference frame. The injection sequence is shown in Fig. 2. The amplitude of the injected signal is 16 V, and the injection period is half of the PWM switching frequency, which is 10 kHz.

TABLE 3. Differential current harmonic content at different maximum speeds.

Maximum speed	Phase	Harmonics	Fundamental frequency	1/3	2/3	1	…	13/3	14/3	5
20 mm/s	A	Amplitude (A)	1.160	7.366E-03	2.330E-03	1.170E-03	…	8.985E-04	1.942E-04	1.745E-04
		Phase angle (°)	0	-25.056	45.830	-44.814	…	84.038	72.311	-158.807
	B	Amplitude (A)	0.104	1.416E-03	7.006E-04	1.654E-03	…	1.207E-04	2.544E-05	2.012E-04
		Phase angle (°)	180	122.651	158.738	-175.335	…	-126.820	151.456	-156.402
200 mm/s	A	Amplitude (A)	1.149	1.256E-02	4.785E-03	2.403E-03	…	1.652E-03	2.660E-04	3.823E-04
		Phase angle (°)	0	-31.127	37.393	62.596	…	79.414	-112.194	4.585
	B	Amplitude (A)	0.102	2.202E-03	7.556E-04	1.720E-03	…	2.102E-04	1.993E-04	1.319E-04
		Phase angle (°)	180	127.915	164.124	-169.072	…	149.805	-37.247	33.442

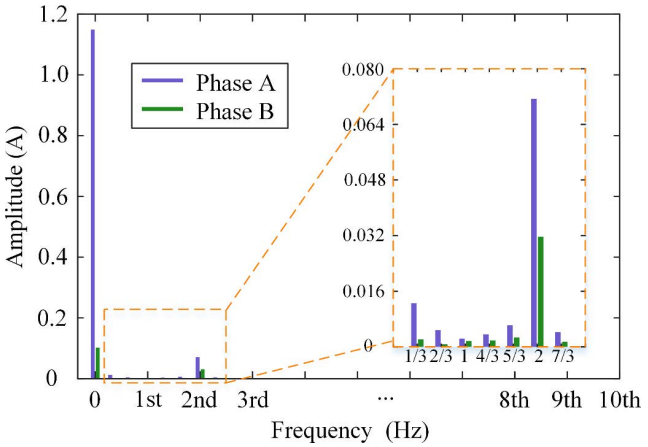

FIGURE 16. Phase A and B differential current FFT spectrum (maximum speed: 200 mm/s).

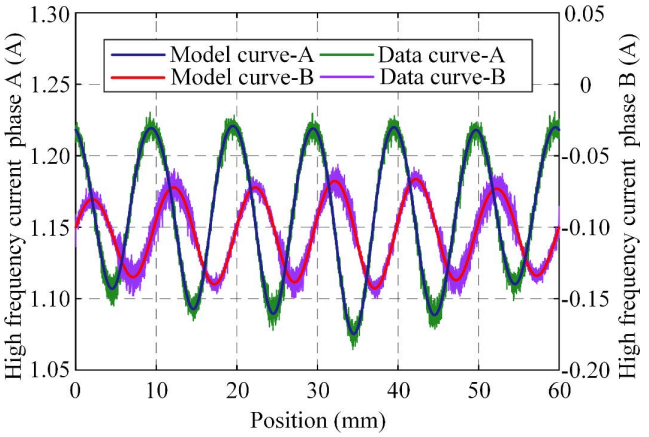

FIGURE 17. Comparison of modeling and measured values (maximum speed: 20 mm/s).

c. Position motion command is applied to the position loop of the servo system, the total displacement is 60 mm, and the type of velocity planning is T-type. Maximum speeds of 20 mm/s and 200 mm/s during the experiment are the maximum values during the acceleration and deceleration processes, respectively.

d. We sampled the currents of the actual phase AB and differentiated them. The sampling period is the same as the PWM period, (i.e., 20 kHz).

e. We performed a difference operation on the high-frequency differential currents obtained in two adjacent PWM cycles in step (4). Operation results are the high differential current signals, as shown in Fig. 13 and Fig. 14.

As shown in Fig. 13 and Fig. 14, with the change of the position of the mover, the currents of the two-phase A and B show a sine wave law, and both have a DC offset. Given that the high-frequency differential current is not a sine wave with a single frequency, it contains numerous harmonic components. In this paper, the FFT is used to analyze the spectral characteristics of the obtained high-frequency differential current, which is used to establish the high-frequency differential current. The current curve model lays the foundation. The specific spectrum analysis results are shown in Fig. 15 and Fig. 16.

The spectrum analysis in Fig. 15 and Fig. 16 show that the high-frequency differential current is mainly composed of fundamental frequency current. Moreover, and the harmonic component is mainly second harmonic, which is consistent with the theoretical analysis result of Equation (19). At the same time, the high-frequency differential current also contains more low-frequency harmonics, including some fractional harmonics. The sampling resolution is 1/3 Hz because the sampling period of linear motor current in the position domain is 20 mm and the sampling length is 60 mm. To better estimate the position, this paper takes the frequency of the first 5 Hz as the frequency distribution range of the model function (i.e., 1/3 Hz to 5 Hz), which is specifically divided into fractional and integer frequencies, as shown in Table 3.

C. HIGH-FREQUENCY CURRENT CURVE MODEL

According to the preceding high-frequency differential current spectrum distribution diagram of the first 5 Hz, the

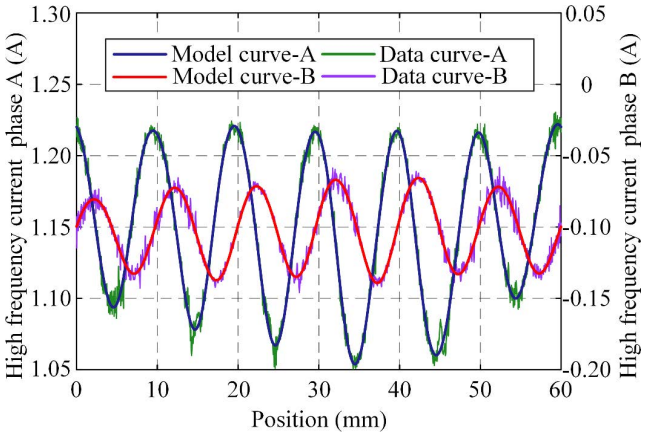

FIGURE 18. Comparison of modeling and measured values (maximum speed: 200 mm/s).

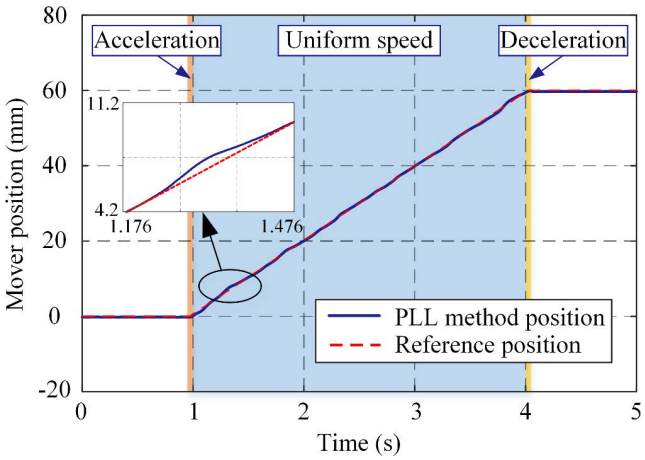

FIGURE 19. PLL method position estimation (20 mm /s).

curve modeling is carried out according to Equation (20). To model the high-frequency differential current obtained at different speeds, so as to realize the Gauss-Newton position iteration method proposed earlier in this study, we convert the high-frequency differential current data from the time-domain coordinate to the position domain coordinate. In the subsequent experimental processing, the methods proposed are carried out in the position domain coordinate.

Evidently, the modeling curve can fit the measured value well. Fig. 17 and Fig. 18 are curve modeling at maximum speeds of 20 mm/s and 200 mm/s, respectively.

D. POSITION ESTIMATION ACCURACY

In the position estimation accuracy experiment, the PLL method in the high-frequency square-waveform injection method and the Gauss-Newton iterative method used in this paper are compared and verified. The experimental process was verified at two maximum speeds of 20 mm/s and 200 mm/s. The velocity planning is T-type acceleration and deceleration. The entire motion process includes five stages: rest, acceleration, uniform speed, deceleration, and stop. The experimental results are shown in Fig. 19 to Fig. 22.

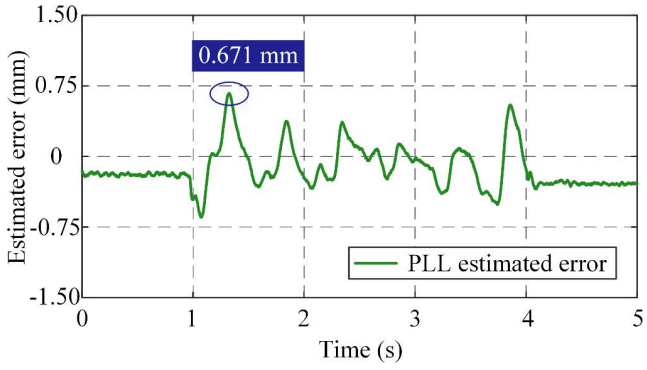

FIGURE 20. PLL method position error (20 mm/s).

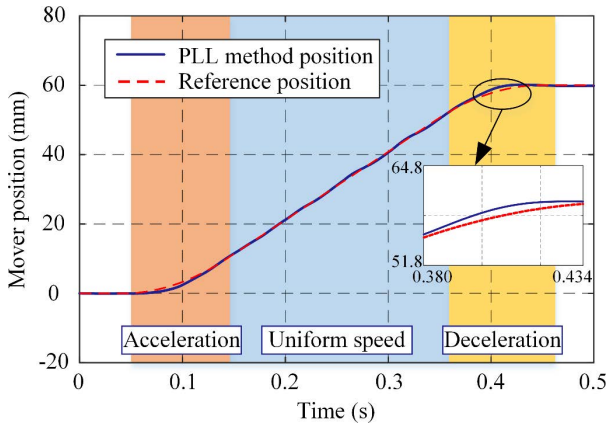

FIGURE 21. PLL method position estimation (200 mm/s).

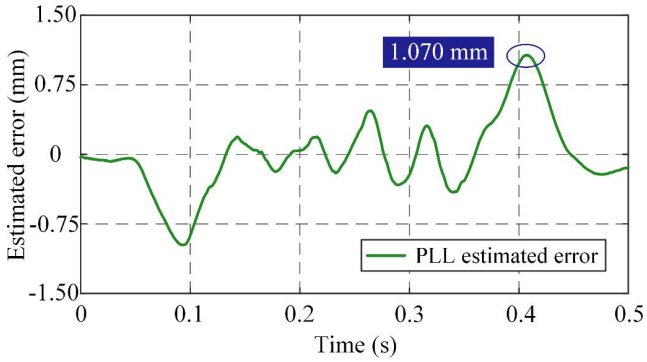

FIGURE 22. PLL method position error (200 mm/s).

As shown in Fig. 20 and Fig. 22, the position estimation accuracies of the PLL method are 0.671 mm and 1.07 mm, respectively. Moreover, the maximum errors at both speeds are near the starting and ending points of the mover motion position. The reason is that in the foregoing analysis, the mover motion starting and ending points are positions with less coupling between the mover and stator (i.e., Fig. 4 represents the partial coupling stage). The fundamental reason for the large error in these two areas is that the amplitude of the high-frequency differential current is affected by the inductance parameters of the motor. In addition, the inductance

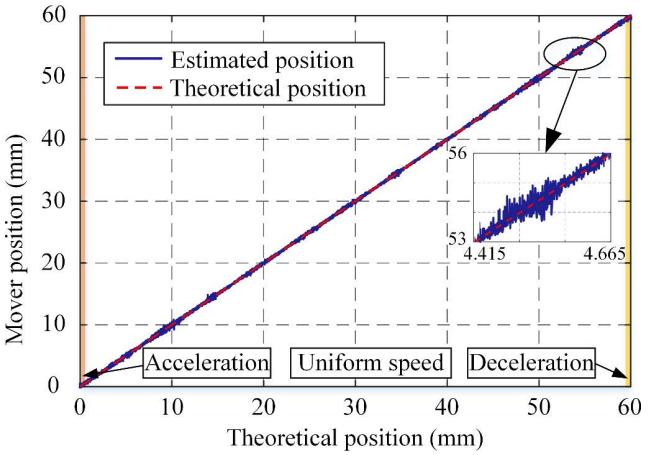

FIGURE 23. Gauss-Newton method position estimation (maximum speed: 20 mm/s).

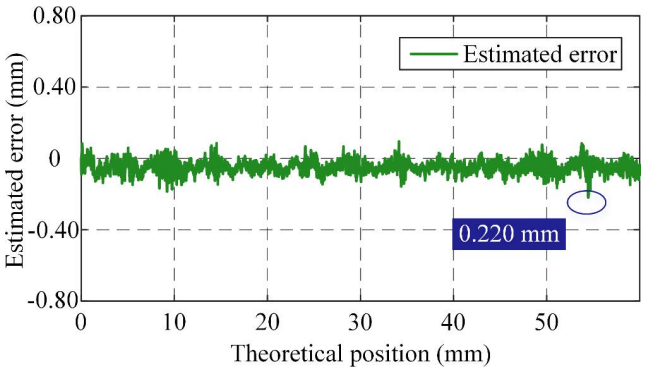

FIGURE 24. Gauss-Newton method position error (maximum speed: 20 mm/s).

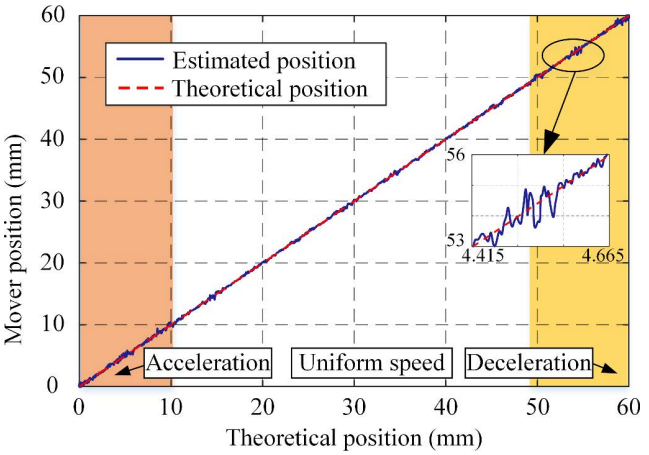

FIGURE 25. Gauss-Newton method position estimation (maximum speed: 200 mm/s).

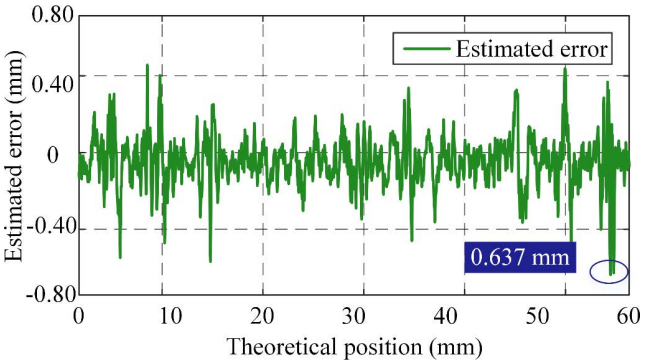

FIGURE 26. Gauss-Newton method position error (maximum speed: 200 mm/s).

TABLE 4. Error comparison of the two methods.

Method	Maximum speed	Maximum error	RMS error	Peak-to-peak error
Gauss-Newton	20 mm/s	0.220 mm	0.0578 mm	0.3146 mm
	200 mm/s	0.637 mm	0.1305 mm	1.0932 mm
PLL	20 mm/s	0.671 mm	0.2557 mm	1.319 mm
	200 mm/s	1.070 mm	0.3998 mm	2.048 mm

parameters will be attenuated to different degrees with the reduction of the coupling length in the partial coupling stage. Therefore, if the existing PLL method is used, then a large position error occurs.

As shown in Fig. 20 and Fig. 22, by comparing errors at two maximum speeds, the position error is shown to be larger when the maximum speed is 200 mm/s. This result is due to the difference in processing the sampled current in the process of extracting the high-frequency differential current. The premise of this processing method is that the fundamental frequency current will not change substantially in two PWM cycles. This method can easily obtain the high-frequency differential current. However, with an increase in movement speed, the fundamental frequency current of PMSLM will change violently. At this time, there will be large errors in the different processing methods, resulting in worse position estimation accuracy when the movement speed is high.

Fig. 23 to Fig. 26 show the position estimation and error analysis, respectively, using the Gauss-Newton iterative method at two maximum speeds. In this part of the experiment, experimental conditions are consistent with the PLL method. that is, the velocity planning is T-type acceleration and deceleration, and maximum speeds are 20 mm/s and 200 mm/s. The motion process at two speeds consists of five stages: rest, acceleration, constant speed, deceleration, and stop. Fig. 24 and Fig. 26 show that the maximum position error is 0.22 mm at a maximum speed of 20 m/s and 0.637 mm at a maximum speed of 200 mm/s, which are 32.7% and 59.5%, respectively, of the PLL method. The position estimation accuracy is substantially improved.

With an increase in speed, the position error increases. Given that this method is also based on high-frequency differential current obtained by the difference method, and the position iterative estimation is carried out on this basis, this

method will inevitably be affected by the change of fundamental frequency current.

Table 4 shows the RMS, maximum, and peak-to-peak error results of the two methods at different maximum speeds. Note that the Gauss-Newton iteration method has a greater improvement in position estimation accuracy than the PLL method.

V. CONCLUSION

In this work, a new high-frequency injection sensorless position estimation method using the Gauss-Newton iteration estimation was investigated. This method is unaffected by the change of coupling length, has strong robustness to the change of the inductance parameters, and can obtain higher position accuracy in the entire stroke. Affected by the change in the coupling length of the mover and stator of the linear motor, the inductance parameters change differently in different coupling stages. In the full coupling stage, it is the second harmonic of the position, and in the partial coupling stage, the amplitude and DC offset attenuation phenomenon occurs. These changes lead to the failure of traditional position sensorless algorithms. The finite element method is used to analyze the variation of the inductance parameters in the entire motion stroke and to verify by the measured values.

In the position estimation process, the high-frequency differential current is obtained by high-frequency square-waveform injection and interpolation processing, and the FFT is performed to obtain the curve model function. The motor has high positional accuracy over the entire travel range. Using this method, experimental verification shows that estimation accuracy is improved by 67.3% and 40.5% compared with the traditional PLL method when the maximum speed of the T-shaped acceleration and deceleration are 20 mm/s and 200 mm/s, respectively. Evidently, the proposed method also causes the drive system to generate acoustic noise. How to reduce the noise requires further research. The proposed method can also be used for the sensorless position estimation of various linear motors.

REFERENCES

[1] I. I. Abdalla, T. Ibrahim, and N. M. Nor, "Analysis of tubular linear motors for different shapes of magnets," *IEEE Access*, vol. 6, pp. 10297–10310, 2018.
[2] Q. Tan, X. Huang, L. Li, and M. Wang, "Research on inductance unbalance and thrust ripple suppression of slot-less tubular permanent magnet synchronous linear motor," *IEEE Access*, vol. 6, pp. 51011–51020, 2018.
[3] F. Cupertino, P. Giangrande, G. Pellegrino, and L. Salvatore, "End effects in linear tubular motors and compensated position sensorless control based on pulsating voltage injection," *IEEE Trans. Ind. Electron.*, vol. 58, no. 2, pp. 494–502, Feb. 2011.
[4] X. Huang, Z. Qian, Q. Tan, J. Li, and B. Zhou, "Suppressing the thrust ripple of the permanent magnet linear synchronous motors with different pole structures by setting the modular primary structures differently," *IEEE Trans. Energy Convers.*, vol. 33, no. 4, pp. 1815–1824, Dec. 2018.
[5] C. Zhang, L. Zhang, X. Huang, J. Yang, and L. Shen, "Research on the method of suppressing the end detent force of permanent magnet linear synchronous motor based on stepped double auxiliary pole," *IEEE Access*, vol. 8, pp. 112539–112552, 2020.
[6] W. Sun, Y. Yu, G. Wang, B. Li, and D. Xu, "Design method of adaptive full order observer with or without estimated flux error in speed estimation algorithm," *IEEE Trans. Power Electron.*, vol. 31, no. 3, pp. 2609–2626, Mar. 2016.
[7] S. Ma, P. Wu, J. Ji, and X. Li, "Sensorless control of salient PMSM with adaptive integrator and resistance online identification using strong tracking filter," *Int. J. Electron.*, vol. 103, no. 2, pp. 217–231, Feb. 2016.
[8] K. D. Hurst, T. G. Habetler, G. Griva, and F. Profumo, "Zero-speed tacholess IM torque control: Simply a matter of stator voltage integration," *IEEE Trans. Ind. Appl.*, vol. 34, no. 4, pp. 790–795, Jul./Aug. 1998.
[9] W. Niwa, Y. Inoue, S. Morimoto, and M. Sanada, "Performance improvement of IPMSM sensorless control in low-speed region using voltage compensation and parameter identification," in *Proc. Int. Power Electron. Conf. (ECCE ASIA)*, Sapporo, Japan, Jun. 2010, pp. 1428–1432.
[10] A. Piippo, M. Hinkkanen, and J. Luomi, "Analysis of an adaptive observer for sensorless control of interior permanent magnet synchronous motors," *IEEE Trans. Ind. Electron.*, vol. 55, no. 2, pp. 570–576, Feb. 2008.
[11] T. Tuovinen, M. Hinkkanen, L. Harnefors, and J. Luomi, "Comparison of a reduced-order observer and a full-order observer for sensorless synchronous motor drives," *IEEE Trans. Ind. Appl.*, vol. 48, no. 6, pp. 1959–1967, Nov. 2012.
[12] J.-I. Ha and S.-K. Sul, "Sensorless field-orientation control of an induction machine by high-frequency signal injection," *IEEE Trans. Ind. Appl.*, vol. 35, no. 1, pp. 45–51, Jan./Feb. 1999.
[13] Y.-D. Yoon, S.-K. Sul, S. Morimoto, and K. Ide, "High-bandwidth sensorless algorithm for AC machines based on square-wave-type voltage injection," *IEEE Trans. Ind. Appl.*, vol. 47, no. 3, pp. 1361–1370, May/Jun. 2011.
[14] Y.-C. Kwon and S.-K. Sul, "Reduction of injection voltage in signal injection sensorless drives using a capacitor-integrated inverter," *IEEE Trans. Power Electron.*, vol. 32, no. 8, pp. 6261–6274, Aug. 2017.
[15] C. Zhang, H. Zhang, P. Ye, and L. Zhang, "Research on sensorless algorithm of two-phase tubular permanent magnet synchronous linear motor," *Trans. China Electrotechn. Soc.*, vol. 34, no. 23, pp. 4901–4908, Dec. 2019.
[16] C. Zhang, P. Ye, and H. Zhang, "Flux linkage and inductance analysis of long-stroke TPMSLM," in *Proc. 22nd Int. Conf. Electr. Mach. Syst. (ICEMS)*, Harbin, China, Aug. 2019, pp. 1–5.
[17] J. M. Liu and Z. Q. Zhu, "Sensorless control strategy by square-waveform high-frequency pulsating signal injection into stationary reference frame," *IEEE J. Emerg. Sel. Topics Power Electron.*, vol. 2, no. 2, pp. 171–180, Jun. 2014.
[18] L. Zhang, B. Li, C. Zhang, H. Zhang, and P. Ye, "Optimization of permanent magnet structure parameters in tubular permanent magnet synchronous linear motor for HF square-wave injection sensorless algorithm," in *Proc. ASME Int. Design Eng. Tech. Conf. Comput. Inf. Eng. (IDETC-CIE)*, 2021, Art. no. V007T07A049.
[19] S.-Y. Jung and K. Nam, "PMSM control based on edge-field Hall sensor signals through ANF-PLL processing," *IEEE Trans. Ind. Electron.*, vol. 58, no. 11, pp. 5121–5129, Nov. 2011.
[20] C. Zhang, H. Zhang, P. Ye, and L. Zhang, "Inductance analysis of two-phase slotless tubular permanent magnet synchronous linear motor," *Trans. China Electrotechn. Soc.*, vol. 36, no. 6, pp. 1159–1168, Mar. 2021.
[21] H. Zhang, B. Kou, L. Wang, Y. Jin, and H. Zhang, "A new inductance measurement method for permanent magnet synchronous linear motor," in *Proc. 17th Int. Conf. Electr. Mach. Syst. (ICEMS)*, Hangzhou, China, Oct. 2014, pp. 1539–1542.

LUHONG ZHANG received the B.S. degree in mechanical engineering and automation from the School of Mechanical Science and Engineering, Jilin University, Jilin, China, in 2016. He is currently pursuing the Ph.D. degree in mechanical engineering with the Department of Mechanical Engineering, Tsinghua University, Beijing, China.

His research interests include linear motor control, servo drive, and sensorless.

BINGRAN LI received the B.S. degree in mechatronics engineering from Shandong University, Shandong, China, in 2015, and the Ph.D. degree in mechanical engineering from Tsinghua University, Beijing, China, in 2020.

He is currently a Postdoctoral Research Fellow with the Department of Mechanical Engineering, Tsinghua University. His current research interests include intelligent numerical control system technology, intelligent control of machine tools, and ultraprecision manufacturing of complex parts.

PEIQING YE received the B.S., M.S., and Ph.D. degrees from the Nanjing University of Aeronautics and Astronautics, Nanjing, China, in 1985, 1988, and 1997, respectively.

He is currently a Professor at the Department of Mechanical Engineering, Tsinghua University, Beijing, China. He has authored or coauthored more than 150 technical articles. He holds more than 40 warranted invention patents. His research interests include computer-aided manufacturing, manufacturing equipment automation, and nontraditional manufacturing process.

CHUNLEI ZHANG received the B.S. degree in mechanical engineering from Tsinghua University, Beijing, China, in 2017, where he is currently pursuing the Ph.D. degree in mechanical engineering.

His research interests include linear motor design motion control and trajectory planning.

HUI ZHANG received the B.S. and Ph.D. degrees in mechanical engineering from the Dalian University of Technology, Dalian, China, in 1992 and 1997, respectively.

She is currently an Associate Professor with the Department of Mechanical Engineering, Tsinghua University, Beijing, China. Her research interests include numerical control and advanced manufacturing technology.